MODEL OF WIND - DRIVEN CIRCULATION IN THE BALTIC SEA

Andrzej Jankowski
Institute of Oceanology of PAS
Sopot, Poland
e-mail: jankowsk@ocean.iopan.gda.pl

Astract
A barotropic H - N model of wind - driven circulation for the Baltic Sea is described. Model is based on the linearized set of the equations of motion with constant eddy viscosity coefficients both the vertical and the lateral. The model has been run on 5 x 5 Nm numerical grid and water movements are forced by surface pressure and wind stress estimatated in standard way. The results of calculations of water circulation due to strong winds of constant velocity as well as due to mean climatic, multi - year averaged, wind fields for selected months are presented. During computations the Baltic was assumed as closed basin i.e. without water exchange through the Danish Sounds and river inflows.

Key words: Baltic sea, barotropic numerical model, wind - driven circulation

1. Introduction

The results of the application of a barotropic numerical model to estimate wind - driven circulation in o the Baltic Sea are described. The non - linear version of the model was adapted to investigate the seiches characteristics in small and shallow water basin (Frischmuth and Jankowski, 1996). The linear baroclinic version of the model was applied in diagnostical studies of mean climatic water circulation in the Baltic Sea (e.g. Jankowski and Kowalik, 1980; Jankowski, 1983; 1996).

The results of the computations are shown in a form of charts of stream function for mass transport and sea level as well as of vectors of the mean - depth and the surface currents.

2 Model description

2.1 Equations and boundary conditions

Model is based on following equations of motion and continuity equation (Ramming and Kowalik, 1980; Simons, 1973):

$$\frac{\partial u}{\partial t} - fv = -\frac{1}{\rho_0}\frac{\partial p}{\partial x} + K_z\frac{\partial^2 u}{\partial z^2} + A_h \cdot \triangle u \tag{1}$$

$$\frac{\partial v}{\partial t} + fu = -\frac{1}{\rho_0}\frac{\partial p}{\partial y} + K_z\frac{\partial^2 v}{\partial z^2} + A_h \cdot \triangle v \tag{2}$$

$$\frac{\partial p}{\partial z} = -\rho_0 g \tag{3}$$

- continuity equation:

$$\frac{\partial u}{\partial x} + \frac{\partial v}{\partial y} + \frac{\partial w}{\partial z} = 0 \tag{4}$$

Initial condition (dla t = 0):

$$u = v = w = p = 0 \tag{5}$$

Boundary conditions at the free sea surface (z = ζ):

$$p = p_a \tag{6}$$

$$\rho_0 K_z\frac{\partial u}{\partial z} = \tau_x^s, \qquad \rho_0 K_z\frac{\partial v}{\partial z} = \tau_y^s \tag{7}$$

$$w_\zeta = \frac{\partial \zeta}{\partial t} + u_\zeta\frac{\partial \zeta}{\partial x} + v_\zeta\frac{\partial \zeta}{\partial y} \tag{8}$$

Boundary conditions at the sea bottom (z = - H):

$$\rho_0 K_z\frac{\partial u}{\partial z} = \tau_x^b, \qquad \rho_0 K_z\frac{\partial v}{\partial z} = \tau_y^b \tag{9}$$

$$w_H = -u_H\frac{\partial H}{\partial x} - v_H\frac{\partial H}{\partial y} \tag{10}$$

where:

u, v, w - components of the current velocity vector along the axes of the Cartesian system of coordinates, the origin of which is located on the free sea surface, the x - axis being oriented to the East, the y - axis to the North

and z - axis vertically, upwards,
$f = 2 \cdot \omega \cdot \sin\varphi$ - Coriolis parameter ($\omega = 0.729 \cdot 10^{-5} rad\ s^{-1}$ angular velocity of the Earth's rotation about its own axis; φ = latitude),
ρ_0 - water density (ρ_0 = const),
K_z - vertical eddy viscosity coefficient (assumed constant with z - axis),
A_h g - acceleration due to gravity,
τ_x^s, τ_y^s - wind stress components at the free sea surface,
τ_x^b, τ_y^b - water shear stress components at the sea bottom,
$u_\zeta, v_\zeta, w_\zeta$ - current velocity vector components at the free sea surface,
u_H, v_H, w_H - current velocity vector components at the sea bottom,
ζ - sea level (ordinate of free sea surface),
p, p_a - hydrostatic and surface atmospheric pressure, respectively,
H - sea depth.

Integration of the hydrostatic equation (3) with respect to z and taking into account boundary conditions (6) for pressure yields:

$$p == p_a + g\rho_0(\zeta - z) \tag{11}$$

Differentiating (11) with respect to x and y and substituting the results into eqs. (1) - (2) we obtain:

$$\frac{\partial u}{\partial t} - fv = -\frac{1}{\rho_0}\frac{\partial p_a}{\partial x} - g\frac{\partial \zeta}{\partial x} + K_z\frac{\partial^2 u}{\partial z^2} + A_h \triangle u \tag{12}$$

$$\frac{\partial v}{\partial t} + fu = -\frac{1}{\rho_0}\frac{\partial p_a}{\partial y} - g\frac{\partial \zeta}{\partial y} + K_z\frac{\partial^2 v}{\partial z^2} + A_h \triangle v \tag{13}$$

2.2 Mass transport and sea level equations

Integrating eqs. (14) - (15) and continuity equation (4) with respect to z from $z = -H$ to $z = \zeta$ and taking into account boundary conditions (7) - (10) we obtain the equations to calculate the mass transport components and sea level:

$$\frac{\partial M_x}{\partial t} - fM_y = -(H+\zeta)\frac{\partial p_a}{\partial x} - \rho_0 g(H+\zeta)\frac{\partial \zeta}{\partial x} + \tau_x^s - \tau_x^b + A_h \triangle M_x \tag{14}$$

$$\frac{\partial M_y}{\partial t} + fM_x = -(H+\zeta)\frac{\partial p_a}{\partial y} - \rho_0 g(H+\zeta)\frac{\partial \zeta}{\partial y} + \tau_y^s - \tau_y^b + A_h \triangle M_y \tag{15}$$

$$\frac{\partial \zeta}{\partial t} + \frac{1}{\rho_0}\left(\frac{\partial M_x}{\partial x} + \frac{\partial M_y}{\partial y}\right) = 0 \tag{16}$$

where:

$$M_x = \int_{-H}^{\zeta} \rho_0 u dz, \quad M_y = \int_{-H}^{\zeta} \rho_0 v dz \quad \text{- mass transport components along the } x\text{-axis and the } y\text{-axis}$$

Pertinent lateral boundary and initial conditions for the mass transport and sea level equations (14) - (16) can be written in a form (Ramming and Kowalik, 1980; Jankowski, 1988):

$$M_n = \begin{cases} 0 & \text{at the closed (solid) boundary,} \\ \Phi(L) & \text{at the open (liquid) boundary.} \end{cases} \tag{17}$$

$$M_\tau = \begin{cases} 0 & \text{at the solid (closed) boundary,} \\ \Phi 1(L) & \text{at the liquid (open) boundary.} \end{cases} \tag{18}$$

$$for \;\; t = 0, \quad \zeta = 0, \quad M_x = 0, \quad ; \; M_y = 0, \tag{19}$$

where:
M_n, M_τ - mass transport vector components, normal and tangential, to lateral boundary L, respectively
$\Phi(L), \Phi 1(L)$ - functions describing water balance at the liquid (open) sea boundary (i.e. river mouth or link with adjacent sea area).

Marchuk and Kagan (1977) proved that the set of eqs. (14) - (16) subject to the boundary (17), (18) and initial (19) conditions, possesses a unique solution; therefore after estimation the external forces and model parameters the set of equations (14) - (16) can be integrated through time to seek out the values of the mass transport components M_x, M_y and ζ in the sea basin area.

2.3 Equation for the horizontal components of the current velocity

For case of stationary atmospheric forcing and disregarding the lateral friction terms in the equations of motion (12) - (13) it can be easy to estimate horizontal currents velocity components. With the above mentioned assumptions eqs. (12), (13) can be rewritten in the form:

$$-fv = -\frac{1}{\rho_0}\frac{\partial p_a}{\partial x} - g\frac{\partial \zeta}{\partial x} + K_z \frac{\partial^2 u}{\partial z^2} \tag{20}$$

$$fu = -\frac{1}{\rho_0}\frac{\partial p_a}{\partial y} - g\frac{\partial \zeta}{\partial y} + K_z \frac{\partial^2 v}{\partial z^2} \tag{21}$$

Assuming that the atmospheric pressure, wind stress components the values of sea level ζ and mass transport components M_x, M_y (from the solution of the set of eqs. (14) - (16)) are known the set of eqs. (20), (21) resolve into an equation for complex velocity $D = u + iv$ (Jankowski, 1988; Ramming and Kowalik, 1980):

$$\frac{\partial^2 D}{\partial z^2} - p_1^2 D = \frac{1}{\rho_0 K_z}(\frac{\partial p_a}{\partial x} + i\frac{\partial p_a}{\partial y}) + \frac{g}{K_z}(\frac{\partial \zeta}{\partial x} + i\frac{\partial \zeta}{\partial y}) \tag{22}$$

where:

$$D = u + iv; \qquad p_1 = \sqrt{\frac{if}{K_z}}; \qquad i = \sqrt{-1} \tag{23}$$

$$\tag{24}$$

Boundary conditions for eq. (22) basing on (7) and (9) can be rewritten in complex form as follows:

$$\text{at } z = \zeta : \qquad \rho_0 K_z \frac{\partial D}{\partial z} = \tau^s = \tau_x^s + i\tau_y^s \tag{25}$$

$$\text{at } z = -H : \qquad \rho_0 K_z \frac{\partial D}{\partial z} = \tau^b = \tau_x^b + i\tau_y^b \tag{26}$$

In the case of constant with z the vertical eddy viscosity coefficient K_z, an analytical, Ekman - type, solution of eq. (22) with boundary conditions (25), (26) may be found out in the form (Jankowski, 1988):

$$D = \frac{\tau^s}{\rho_0 K_z p_1}\frac{cosh[p_1(H+z)]}{sinh[p_1(H+\zeta)]} - \frac{\tau^b}{\rho_0 K_z p_1}\frac{cosh[p_1(z)]}{sinh[p_1(H+\zeta)]} + \frac{g}{if}(\frac{\partial \zeta}{\partial x} + i\frac{\partial \zeta}{\partial y}) + \frac{1}{\rho_0 if}(\frac{\partial p_a}{\partial x} + i\frac{\partial p_a}{\partial y}) \tag{27}$$

where:

$$\tau^s = \tau_x^s + i\tau_y^s; \quad \tau^b = \tau_x^b + i\tau_y^b; \tag{28}$$

Introducing into (27) the values of sea level ζ and mass transport components M_x, M_y from the solution of the set of eqs. (14) - (16) and estimates of model parameters: i.e. the components of tangential wind stress τ_x^s, τ_y^s and bottom stress τ_x^b, τ_y^b, and the vertical eddy viscosity coefficient K_z one can calculate the horizontal components of the current velocity vector.

2.4 Model parameters and atmospheric forcing

Tangential wind stress components τ_x^s, τ_y^s and tangential bottom water stress components τ_x^b, τ_y^b were calculated by well tested formulae used in hydrodynamical - numerical models (Simons, 1973; Ramming and Kowalik, 1980; Kowalik and Murty, 1993; Jankowski, 1988):
- wind stress components:

$$\tau_x^s = \rho_a C_D W_a W_x, \qquad \tau_y^s = \rho_a C_D W_a W_y. \tag{29}$$

- bottom shear water stress components:

$$\tau_x^b = RM_x, \qquad \tau_y^b = RM_y, \qquad R = \frac{r}{(H+\zeta)^2}\sqrt{M_x^2 + M_y^2}. \tag{30}$$

where:
$W_a = \sqrt{W_x^2 + W_y^2}$ - absolute value of wind vector velocity,
W_x, W_y - components of wind vector velocity,
ρ_a, C_D - air density and drag coefficient, respectively,
r - bottom friction coefficient.

In our calculations the standard values for air density $\rho_a = 1.3{\cdot}10^{-3} g/cm^3$, for drag coefficient $C_D = 2.6 \cdot 10^{-3}$ and for the bottom friction coefficient $r = 2.5 \cdot 10^{-3}$, usually used in numerical calculations of storm surges and water circulation in the natural basins (Simons, 1973; Ramming and Kowalik, 1980), were applied.

For the case of mean climatic, multi - year averaged atmospheric forcing, first the geostrophic wind was determined from the distribution of atmospheric pressure:

$$W_a = C_r W_{ag} = C_r B_T \frac{\partial p_a}{\partial n} \tag{31}$$

where:
W_{ags} W_{ag} - module of geostrophic (gradient) wind vector velocity,
$C_r = 0.7$ - reduction factor,taking into account weakening of wind velocity due to friction effects in vicinity of the free sea surface,
$\frac{\partial p_a}{\partial n}$ - horizontal gradient of atmospheric pressure (in hPa/100 km),
B_T - coefficient including the stratification conditions at the sea - atmosphere interface (assumed constant and equal to 4.69, i.e. mean value of data being taken from Garbalewski and Malicki (1971)).

Next wind stress components are estimated by standard formulas (29) mentioned above with $W_a = W_{ags}$ and taking into account deflection angle between the geostrophic surface wind W_{ags} and "real" surface wind W_a α

equal to 15^o (in counterclockwise direction) (Jankowski, 1988; Svansson, 1972).

The eddy viscosity coefficient K_z was estimated by the Felsenbaum's theory of wind - driven currents, in which values of K_z, depended on wind velocity, Coriolis parameter and basin depth can be estimated by expressions (Ramming and Kowalik, 1980; Jankowski, 1988; Svansson, 1972):

$$K_z = \alpha_1 W_a H; \quad if \quad H < H_{cr} \quad or \quad K_z = \alpha_2 \frac{W_a^2}{f}; \quad if \quad H \geq H_{cr} \tag{32}$$

where:
$H_{cr} = \alpha_3 W_a / f$ - critical depth,
$\alpha_1, \alpha_2, \alpha_3$ - coefficients equal to: $0.54 \cdot 10^{-4}$, $4.7 \cdot 10^{-8}$, $8.7 \cdot 10^{-4}$, respectively.

The coefficient of the lateral eddy viscosity (the lateral friction coefficient) A_h as it is been found out (cf. Defant, 1961; Ozmidov, 1968) is dependent on spatial scale of the dynamic processes and in general satisfies the Richardson law:

$$A_h = c_0 \cdot L^{4/3} \tag{33}$$

where: L denotes the horizontal scale of the turbulent eddies, and c_0 - an empirical constant of proportionality with an order of magnitude of $0.01 cm^{2/3}/s$ (cf. Ozmidov, 1968).

In shallow water basin the influence (role) of the lateral friction from physical point of view is minor comparing to bottom friction, but because of bottom variability and irregularity of the shore line one can include the lateral friction terms into numerical model treate them as smoothing terms, to filter out the parasite instabilties generated during numerical computations due to above mentioned variabilities of the bottom relief and coast line.

In the model calculations the lateral eddy viscosity was estimated by formula (33) with the horizontal scale L egual to several space steps of numerical grid. After some experiments the final computations were carried out with the value of the lateral coefficient of order of A_h ($5 \cdot 10^7 cm^2/s$).

3. Numerical method of solution of mass transport and sea level equations

The finite explicite difference scheme used by Hansen (Hansen, 1962: Ramming and Kowalik, 1980) was applied to the system of eqs. (14) -(16), and the numerical calculations were carried out with time step equal to 60 seconds and space steps equal to $h_x = h_y = h = 5Nm$. The locations of the calculated variables on the finite difference grid (Arakawa C - grid) are depicted in Fig. 1 and the layout of numerical grid points in xyz - plane are shown in Fig. 2.

Finite difference form of equations for mass transport and sea level (14) - (16) is as follows (Ramming and Kowalik, 1980; Kowalik and Murty, 1993):

$$M_{x_{m+1,n}}^{t+\tau} = (1 - 2\overline{R_{m+1,n}}\tau)M_{x_{m+1,n}}^{t-\tau} + 2f\tau\overline{M_y} + 2\tau G_{x_{m+1,n}} - \rho_0 g H_{m+1,n}\frac{\tau}{h_x}(\zeta_{m+2,n}^t - \zeta_{m,n}^t),$$
$$+A_h\frac{\tau}{2h_x^2}(M_{x_{m+1,n+2}}^{t-\tau} + M_{x_{m+1,n-2}}^{t-\tau} + M_{x_{m+3,n}}^{t-\tau} + M_{x_{m-1,n}}^{t-\tau} - 4M_{x_{m+1,n}}^{t-\tau}) \quad (34)$$

$$M_{y_{m,n+1}}^{t+\tau} = (1 - 2\overline{R_{m,n+1}}\tau)M_{y_{m,n+1}}^{t-\tau} - 2f\tau\overline{M_x} + 2\tau G_{y_{m,n+1}} - \rho_0 g H_{m,n+1}\frac{\tau}{h_y}(\zeta_{m,n+2}^t - \zeta_{m,n}^t),$$
$$+A_h\frac{\tau}{2h_y^2}(M_{y_{m+2,n+1}}^{t-\tau} + M_{y_{m-2,n+1}}^{t-\tau} + M_{y_{m,n+3}^{t-\tau}}^{t-\tau} + M_{y_{m,n-1}}^{t-\tau} - 4M_{y_{m,n+1}}^{t-\tau}) \quad (35)$$

$$\zeta_{m,n}^{t+2\tau} = \zeta_{m,n}^t - \frac{\tau}{\rho_0 h_y}(\frac{1}{h_x}(M_{x_{m+1,n}}^{t+\tau} - M_{x_{m-1,n}}^{t+\tau}) + \frac{1}{h_y}(M_{y_{m,n+1}}^{t+\tau} - M_{y_{m,n-1}}^{t+\tau})). \quad (36)$$

where:

$$G_{x_{m+1,n}} = H_{m+1,n}\frac{(p_{a_{m+2,n}} - p_{a_{m,n}})}{2h_x} + \tau_{x_{m+1,n}}^s, \quad (37)$$

$$G_{y_{m,n+1}} = H_{m,n+1}\frac{(p_{a_{m,n+2}} - p_{a_{m,n}})}{2h_y} + \tau_{y_{m,n+1}}^s, \quad (38)$$

$$\overline{M_y} = 0.25(M_{y_{m+2,n+1}}^{t-\tau} + M_{y_{m+2,n-1}}^{t-\tau} + M_{y_{m,n+1}}^{t-\tau} + M_{y_{m,n-1}}^{t-\tau}) \quad (39)$$

$$\overline{M_x} = 0.25(M_{x_{m+1,n+2}}^{t-\tau} + M_{x_{m-1,n+2}}^{t-\tau} + M_{x_{m+1,n}}^{t-\tau} + M_{x_{m-1,n}}^{t-\tau}) \quad (40)$$

$$\overline{R_{m+1,n}} = \frac{r}{[H + 0.5(\zeta_{m+2,n}^t + \zeta_{m,n}^t)]^2}\sqrt{(M_{x_{m+1,n}}^{t-\tau})^2 + \overline{M_y}^2} \quad (41)$$

$$\overline{R_{m,n+1}} = \frac{r}{[H + 0.5(\zeta_{m,n+2}^t + \zeta_{m,n}^t)]^2}\sqrt{\overline{M_x}^2 + (M_{y_{m,n+1}}^{t-\tau})^2} \quad (42)$$

Stability condition for above the finite difference scheme are as follows (this similar to standard CFL's criterion) (Ramming and Kowalik, 1980; Kowalik and Murty, 1993):

$$\tau \leq \frac{h}{\sqrt{2gH_{max}}} \quad (43)$$

where:
H_{max} - maximal basin depth,
τ - time step,
h - space step: $h = max(h_x, h_y)$
h_x, h_y - space steps of the H-N numerical grid along the x -axis
and y - axis, respectively.

Results and comments

The model set up on the cartesian square numerical grid covering the Baltic Sea area on the sea map in the Mercator projection (basic coordinate lines: 19^o E and 60^o N, respectively).

Bottom topography of the Baltic Sea for the numerical model was smoothed and Fig. 3 shows final form of the bottom relief of the sea basin used in the model computations.

In Figs. 4 and 5 the calculated wind velocity vectors fields for selected months are presented as well as the multi - year atmospheric surface pressure.

Figs. 6 - 13 display distributions of stream function for mass transport, sea level, mean - depth currents and suface currents for the selected months calculated by the model.

Figs. 14 - 21 present results of calculations of stream function, sea level, mean - depth currents and surface currents for the case of strong winds of constant velocity equal to 10 m/s blowing from basic wind directions.

Stream function Ψ was calculated from the mass transport components M_x, M_y by means of the steady - state form of sea level equation (16) and the standard formulas:

$$M_x = -\frac{\partial \Psi}{\partial y}; \qquad M_y = \frac{\partial \Psi}{\partial x} \tag{44}$$

The spatial distributions of the circulational characteristics for the mean, multi - year averaged, wind fields for selected months (Figs. 6 - 13) as well as for strong wind (Figs. 14 - 21) are well correlated with the atmospheric forcing and the Baltic Sea morphometry. The basics features of circulation - cyclonic and anticyclonic gyres are located in the regions of the Baltic Sea with the specific bottom relief and shore line structures (deeps, furrows and banks, bays etc.).

The estimated wind - driven circulation patterns show the essential influence of the bottom relief and the complex coast lines of the basin on the calculated circulational characteristics and they confirm the results of the other investigaters (e.g. Kowalik and Sta/skiewicz, 1976; Simons, 1978; Kielmann, 1981; Mälkki and Tamsalu, 1975; Krauss and Brügge, 1991).

Water circulation in the Baltic Sea, which is controlled by the complex coast lines and bottom relief and driven by the wind and the thermohaline forcing (the last not considered in the presented calculations), may have some influence on the distributions of ecological, biological or pollution fields.

Presented patterns of the wind - driven circulation in the barotropic Baltic Sea may serve as the hydrological background for understanding of variability of the ecological parameters giving the overall picture of sea water dynamics in barotropic case.

References

Defant A.I., 1961, *Physical oceanography*, vol. 1, Pergamon Press, Oxford, London, Paris, New York, 729 pp.

Frischmuth K., Jankowski A., 1996, *Estimation of period of free oscillations (seiches) in the Kirrbucht.* Oceanologia, No. 38 (4), 503 - 526,

Garbalewski C., Malicki J., 1971, *Influence of thermal stratification of the lower atmosphere and water temperature on wind velocity above the Baltic.* Wiadomo/sci S/lu/zby Hydrol. i Meteorol., 7 (19), 37-46 (in Polish)

Hansen W., 1962, *Hydrodynamical methods applied to oceanographic problems.* Proc.Sympos. Mathem. - Hydrodyn. Methods of Phys. Oceanography, Hamburg, 25 - 34

Jankowski A., 1983b, *An model H-N for the calculation of wind - and density - driven circulation in the Baltic Sea.* Part II. *Density - driven circulation in the summer season.* Oceanologia, No. 16, 17-40

Jankowski A., 1988, *Mathematical modelling of water circulation in the Baltic Sea.* Seria "Prace habilitacyjne", Ossolineum, Wroc/law 1988, 1 - 281 (in Polish)

Jankowski A., 1996, *Vertical water circulation in the southern Baltic Sea and its environmental implications.*, Oceanologia, No. 38 (4), 483 - 501,

Jankowski A., Kowalik Z., 1980, *Diagnostic model of wind - and density - driven currents in the Baltic Sea.* Oceanologica Acta, vol. 3, No. 3, 301-308

Kielmann J., 1981, *Grundlagen und Anwendung eines numerischen Modells der geschichen Ostsee.*, Ber. Inst. Meereskunde Universität Kiel, 87a, b

Kowalik Z., Murty T.S., 1993, *Numerical modeling of ocean dynamics*, Advanced Series on Ocean Engineering - Vol. 5, World Scientific, Singapore - New Jersey - London - Hong Kong, 1993, 481 pp.

Kowalik Z., Sta/skiewicz A., 1976, *Diagnostic model of the circulation in the Baltic Sea.*, Dt. hydrogr. Z., 29, No. 6, 239 - 250

Marchuk G.I., Kagan B.A., 1977, *Ocean tides.* Gidrometeoizdat, Leningrad, 296 pp. (in Russian)

Mälkki P., Tamsalu R., 1985 *Physical features of the Baltic Sea*. Finnish Marine Research, 252, 109pp.

Ozmidov R.V., 1968, *Horizontal turbulence and turbulent exchange in the ocean* , Isdat. Nauka, Moskva, 200 pp. (in Russian)

Ramming H.G., Kowalik Z., 1980, *Numerical modelling of marine hydrodynamics.* Elsevier Oceanography Series, 26, 1980, 369 pp.

Simons T.J., 1973, *Development of three - dimensional numerical models of the Great Lakes*, Inland Water Directoriate Scientific Series No. 12, Canada Centre for Inland Waters, Burlington, Ontario, 1973, 26 pp.

Simons T.S., 1978, *Wind - driven circulations in the southwest Baltic.* Tellus, 30, 272 - 283

Svansson A., 1972, *Canal models of sea level and salinity variations in the Baltic and adjacent waters.*, Series Hydrography, Rap. No. 26, Fishery Board of Sweden, 72 pp.

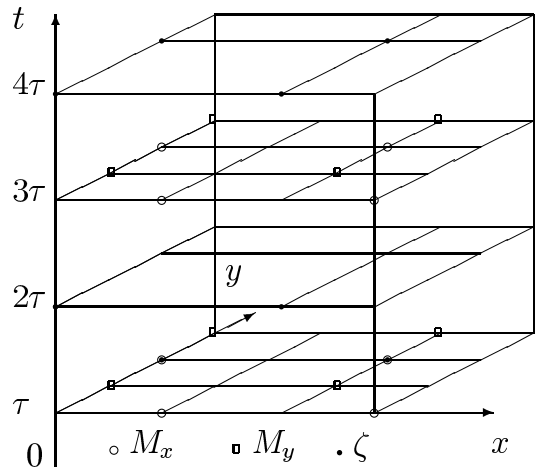

Fig. 1 The H-N numerical grid in the x - y - t - space

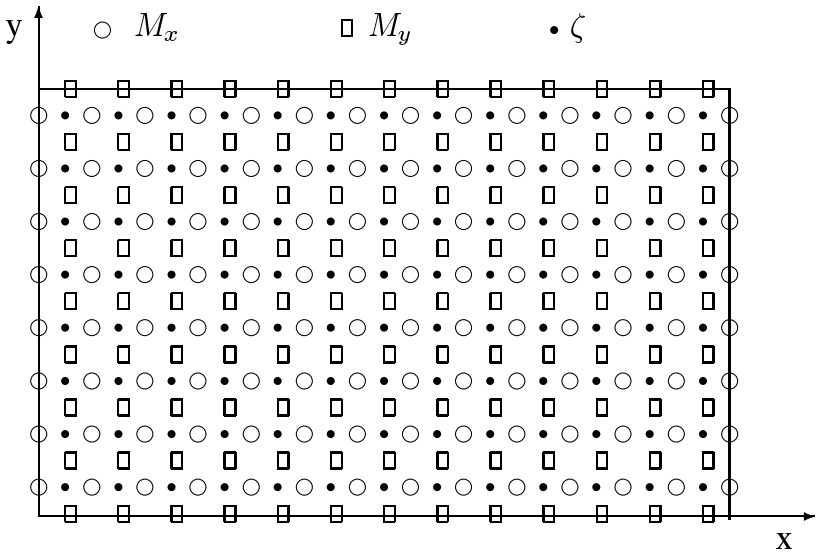

Fig. 2 The H-N numerical grid in the x - y plane

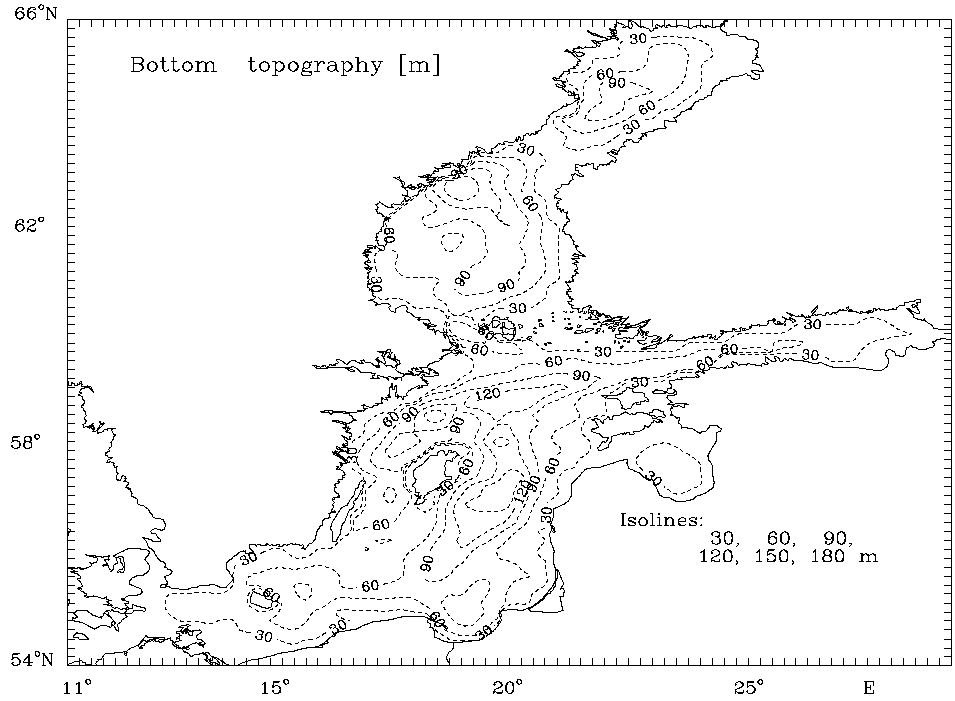

Figure 3: Bottom topography [m] of the Baltic Sea used in the model

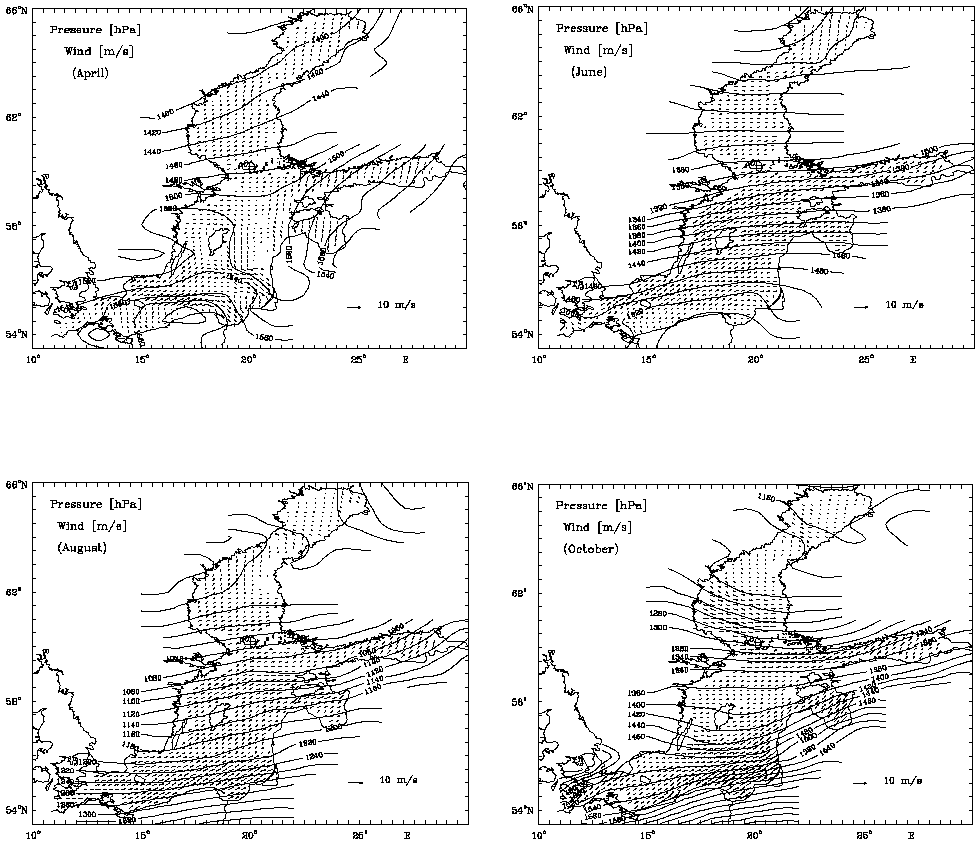

Figure 4: The multi-year averaged surface atmospheric pressure anomaly [hPa] and the calculated quasi-geostrophic wind field [m/s] selected months: April, June, August and October.

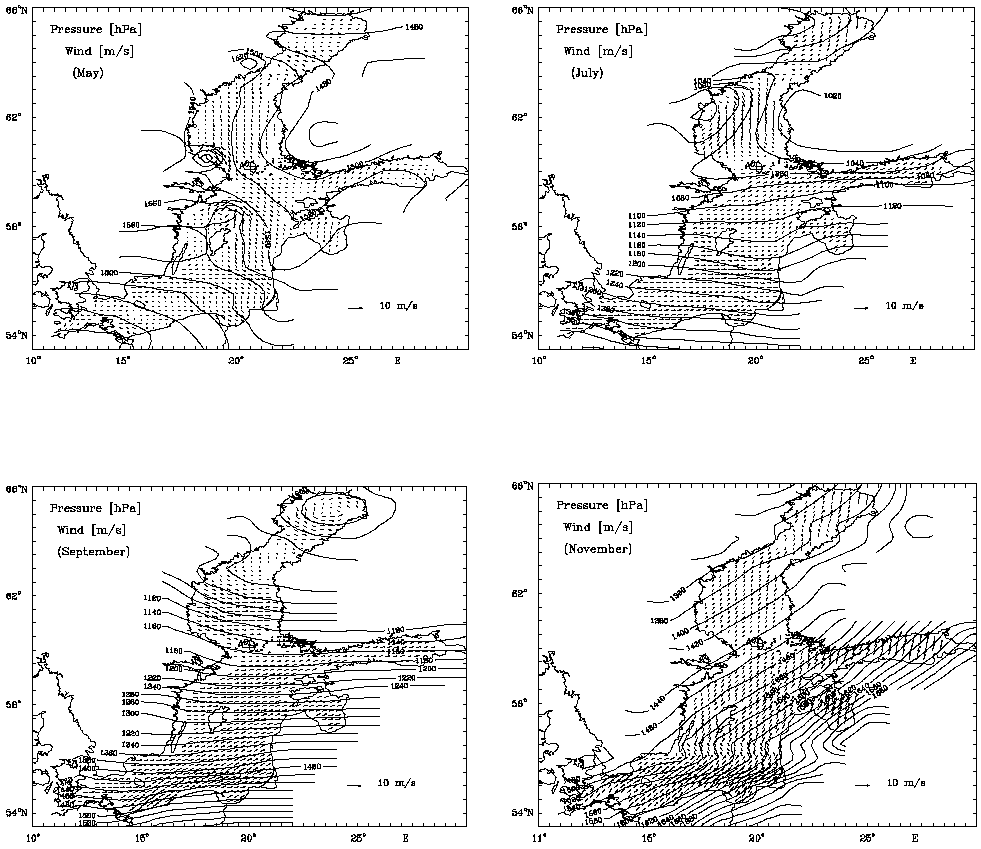

Figure 5: The multi-year averaged surface atmospheric pressure anomaly [hPa] and the calculated quasi-geostrophic wind field [m/s] selected months: May, July, September and November.

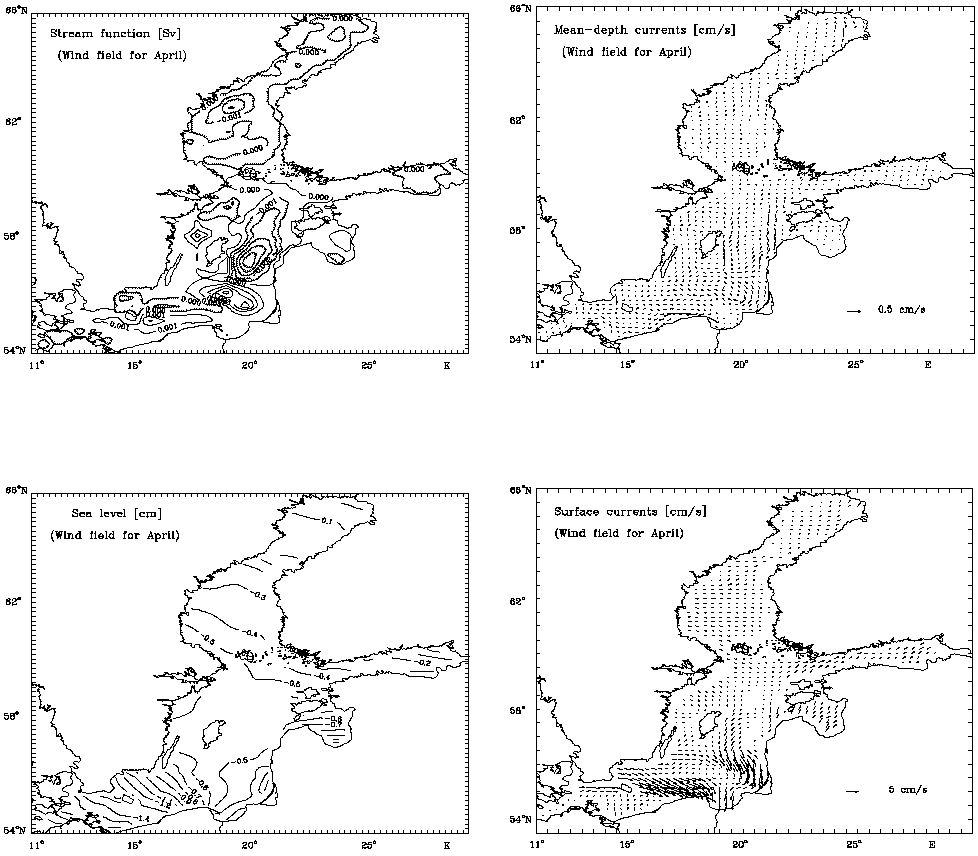

Figure 6: Stream function for mass transport [Sv], mean - depth currents [cm/s], sea level [cm] and surface currents [cm/s] for selected months: April. The hatched areas in stream function distributions indicate the regions of counterclockwise (cyclonic) water circulation.

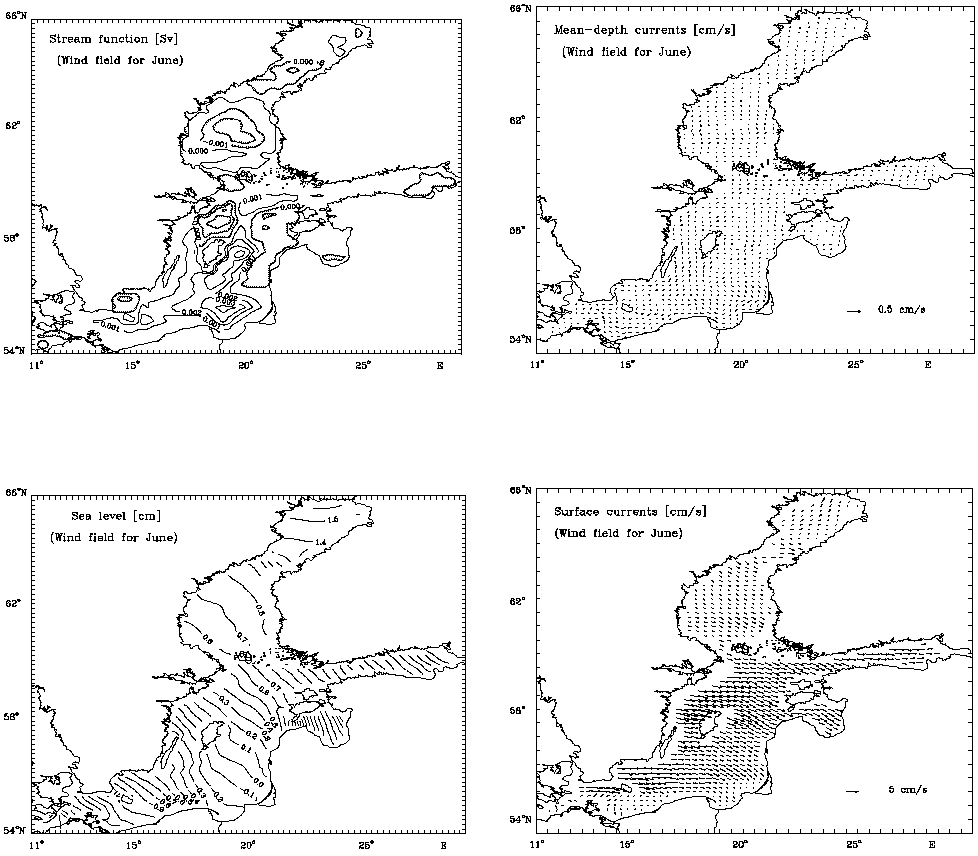

Figure 7: Stream function for mass transport [Sv], mean - depth currents [cm/s], sea level [cm] and surface currents [cm/s] for selected months: June. The hatched areas in stream function distributions indicate the regions of counterclockwise (cyclonic) water circulation.

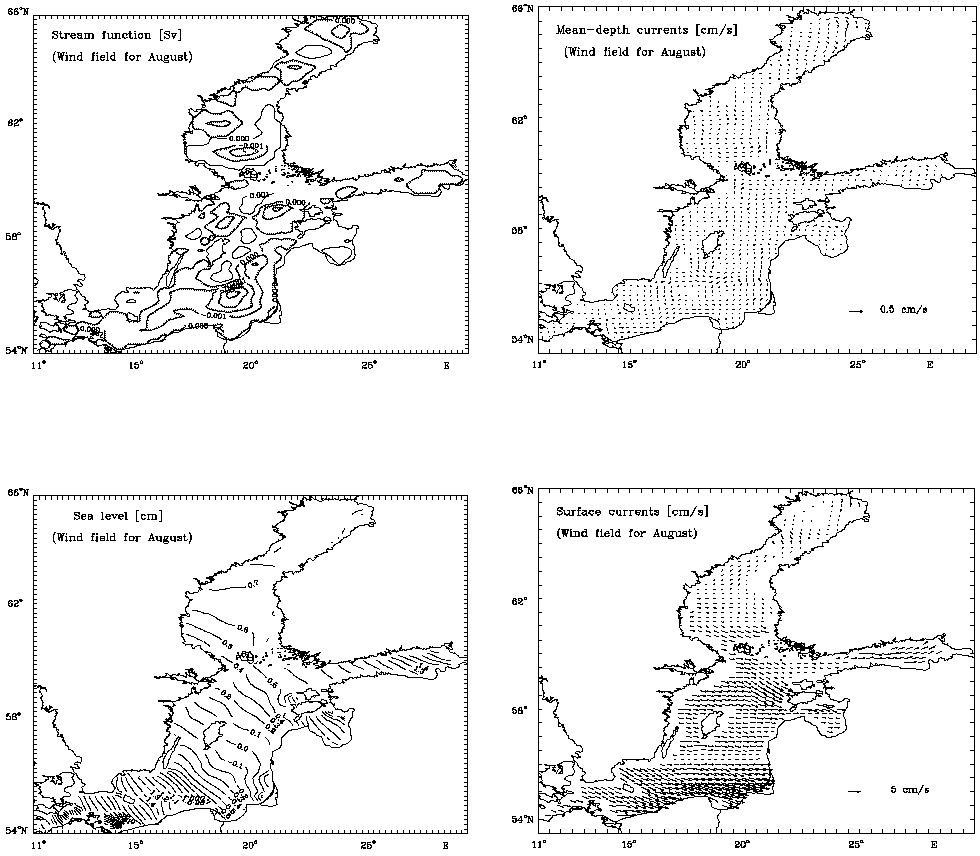

Figure 8: Stream function for mass transport [Sv], mean - depth currents [cm/s], sea level [cm] and surface currents [cm/s] for selected months: August. The hatched areas in stream function distributions indicate the regions of counterclockwise (cyclonic) water circulation.

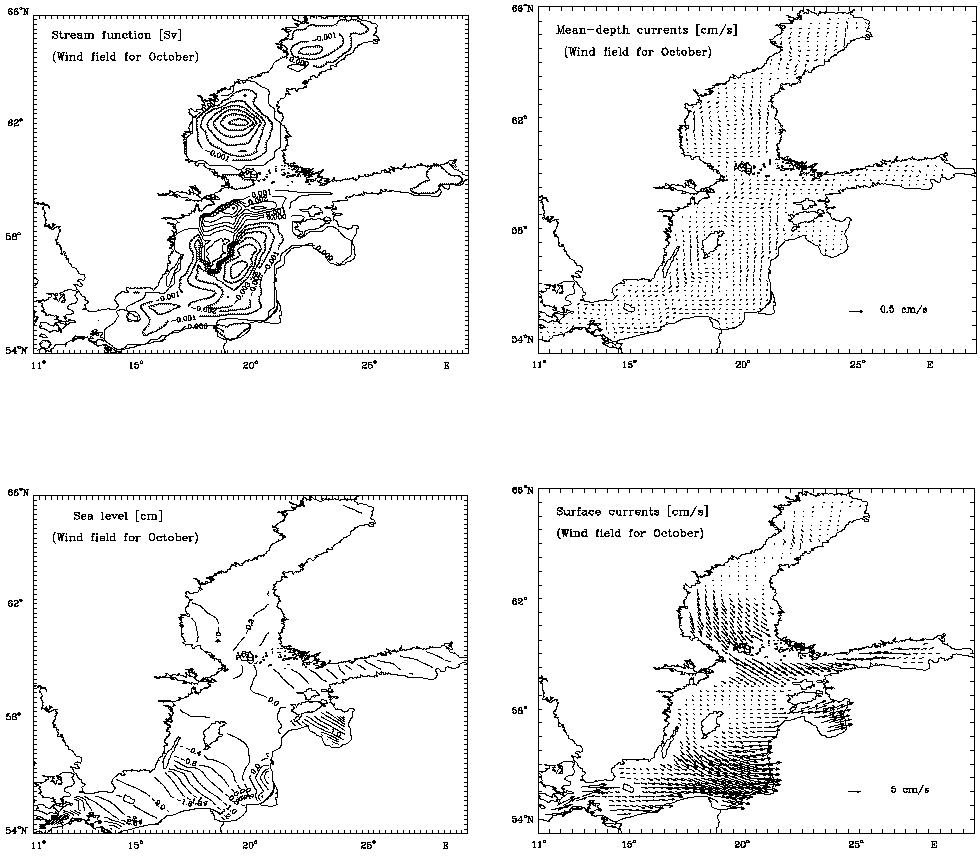

Figure 9: Stream function for mass transport [Sv], mean - depth currents [cm/s], sea level [cm] and surface currents [cm/s] for selected months: October. The hatched areas in stream function distributions indicate the regions of counterclockwise (cyclonic) water circulation.

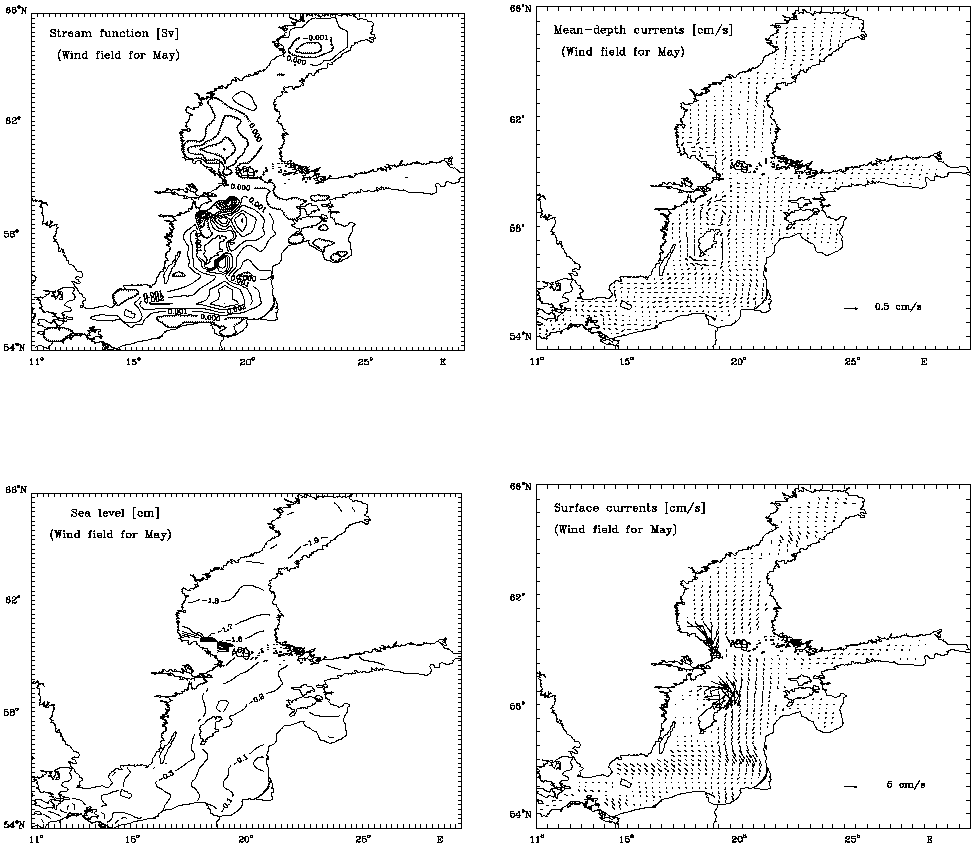

Figure 10: Stream function for mass transport [Sv], mean - depth currents [cm/s], sea level [cm] and surface currents [cm/s] for selected months: May. The hatched areas in stream function distributions indicate the regions of counterclockwise (cyclonic) water circulation.

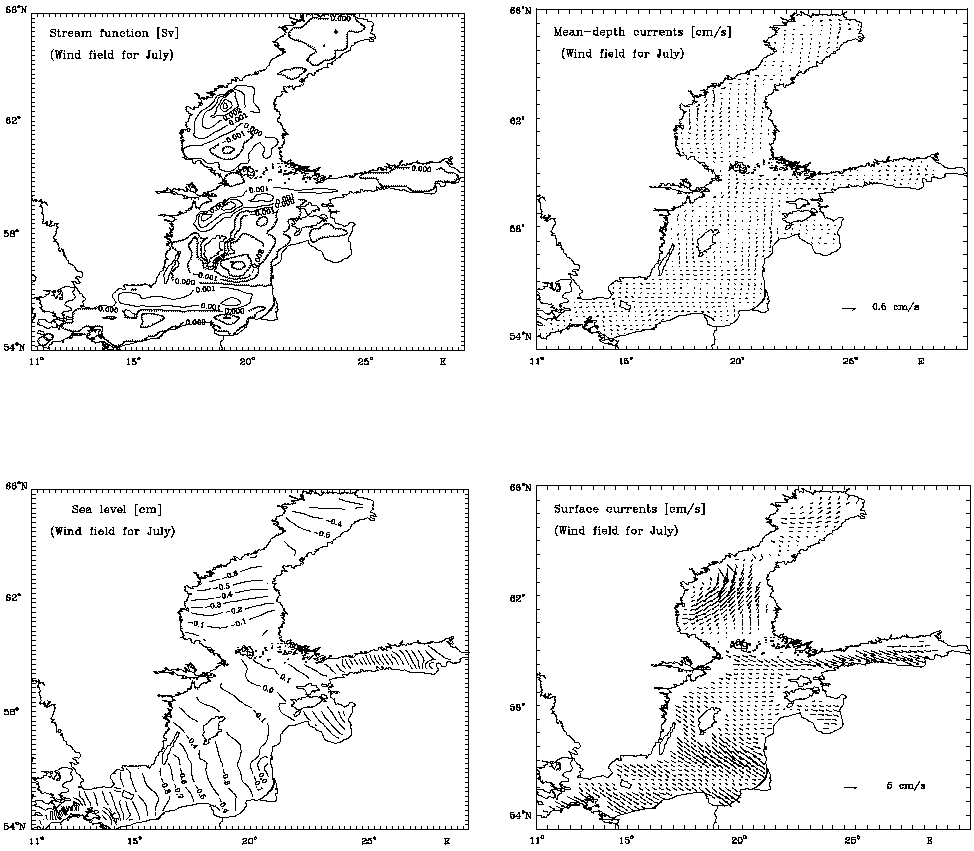

Figure 11: Stream function for mass transport [Sv], mean - depth currents [cm/s], sea level [cm] and surface currents [cm/s] for selected months: July. The hatched areas in stream function distributions indicate the regions of counterclockwise (cyclonic) water circulation.

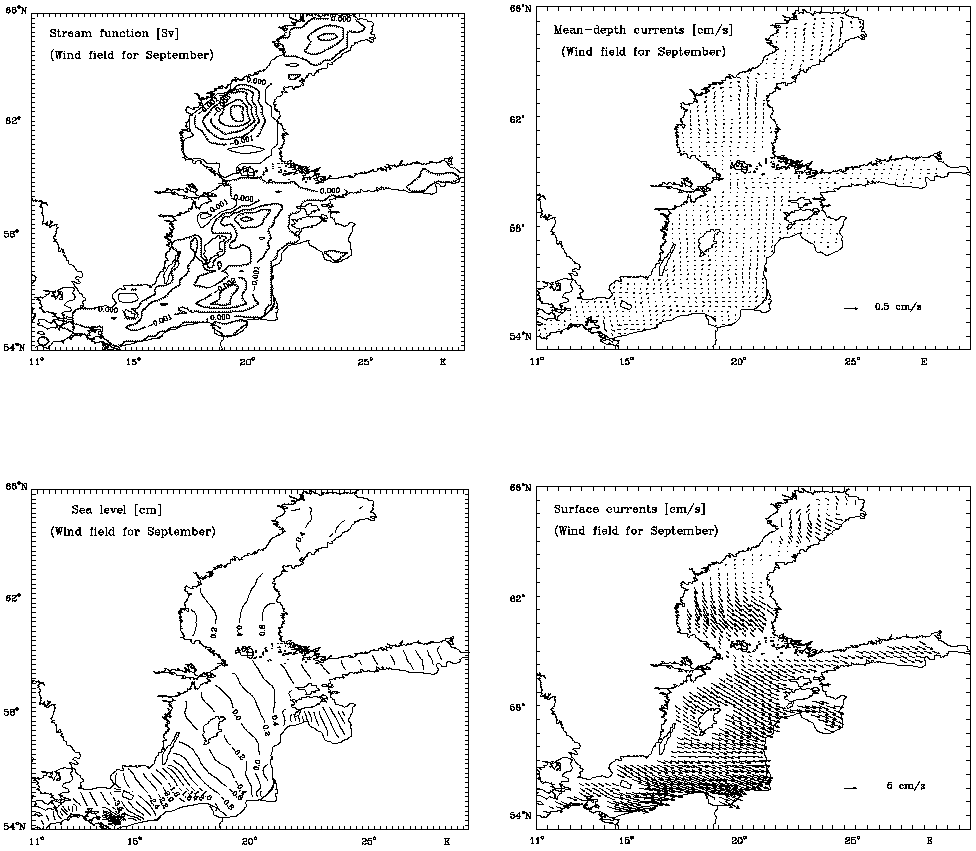

Figure 12: Stream function for mass transport [Sv], mean - depth currents [cm/s], sea level [cm] and surface currents [cm/s] for selected months: September. The hatched areas in stream function distributions indicate the regions of counterclockwise (cyclonic) water circulation.

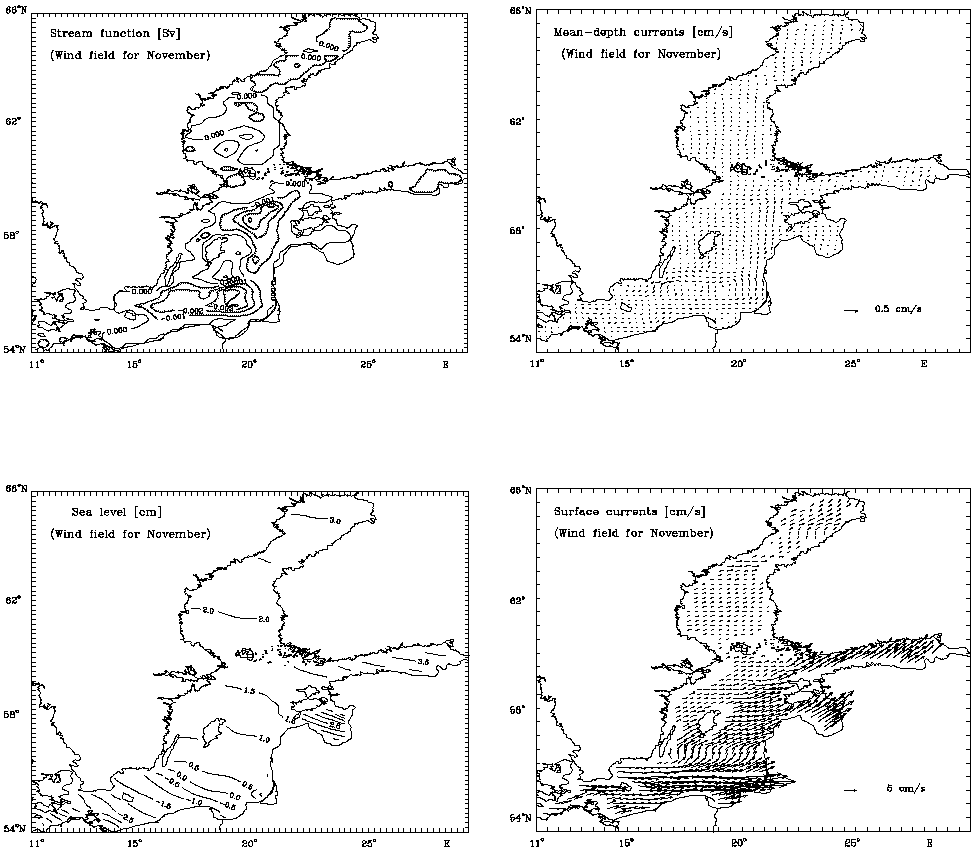

Figure 13: Stream function for mass transport [Sv], mean - depth currents [cm/s], sea level [cm] and surface currents [cm/s] for selected months: November. The hatched areas in stream function distributions indicate the regions of counterclockwise (cyclonic) water circulation.

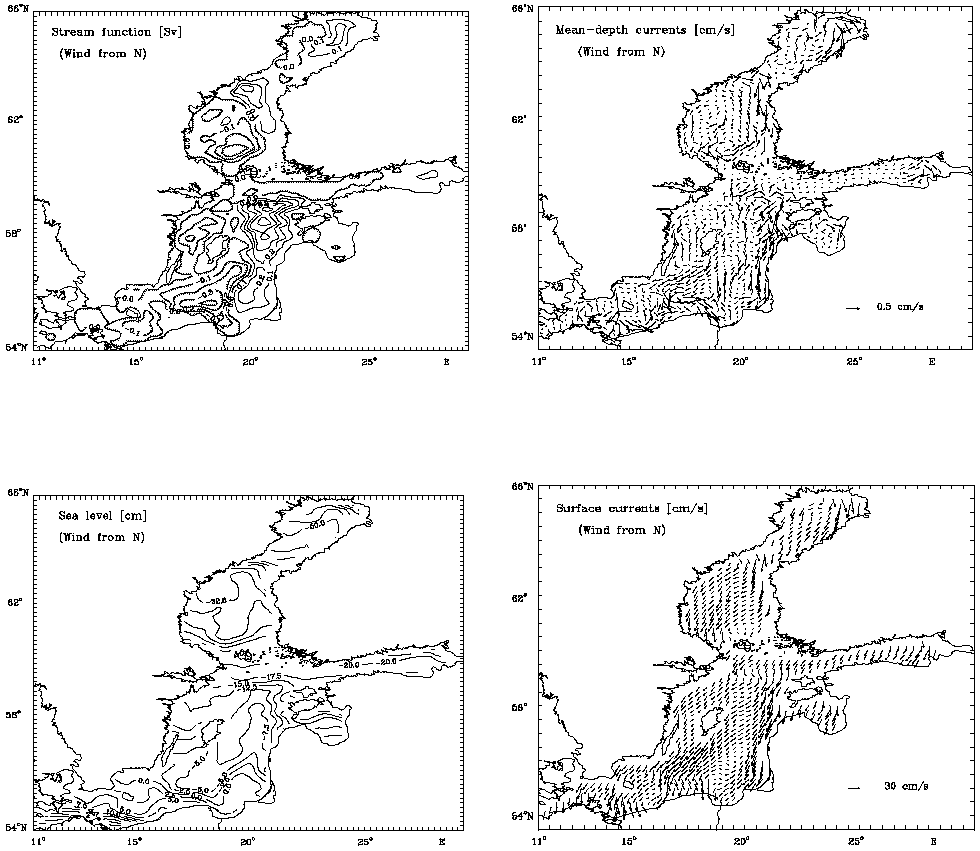

Figure 14: Stream function for mass transport [Sv], mean - depth currents [cm/s], sea level [cm] and surface currents [cm/s] for the strong wind of constant velocity blowing from North. The hatched areas in stream function distributions indicate the regions of counterclockwise (cyclonic) water circulation.

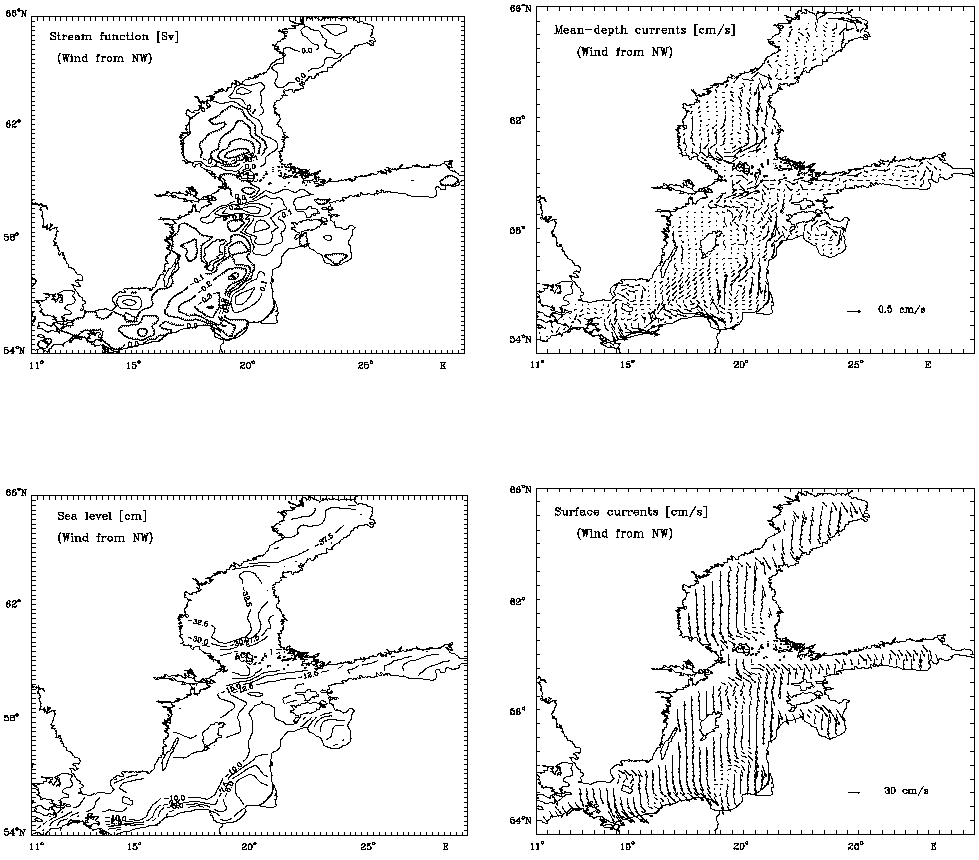

Figure 15: Stream function for mass transport [Sv], mean - depth currents [cm/s], sea level [cm] and surface currents [cm/s] for the strong wind of constant velocity blowing from Northwest. The hatched areas in stream function distributions indicate the regions of counterclockwise (cyclonic) water circulation.

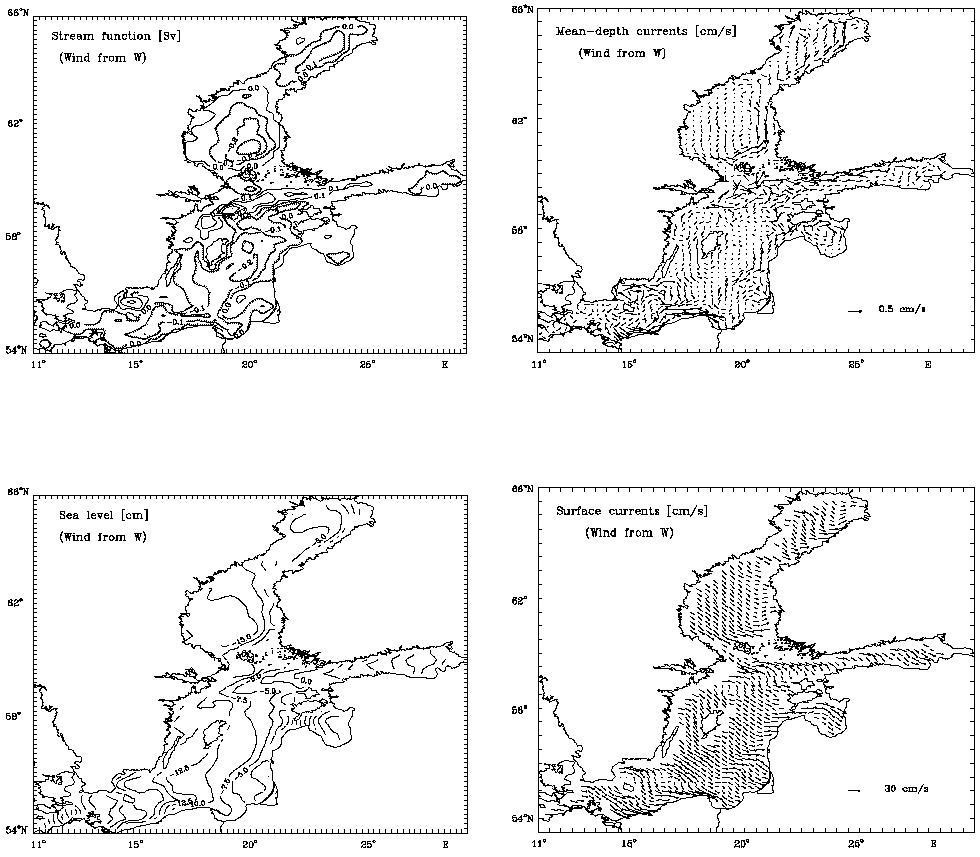

Figure 16: Stream function for mass transport [Sv], mean - depth currents [cm/s], sea level [cm] and surface currents [cm/s] for the strong wind of constant velocity blowing from West. The hatched areas in stream function distributions indicate the regions of counterclockwise (cyclonic) water circulation.

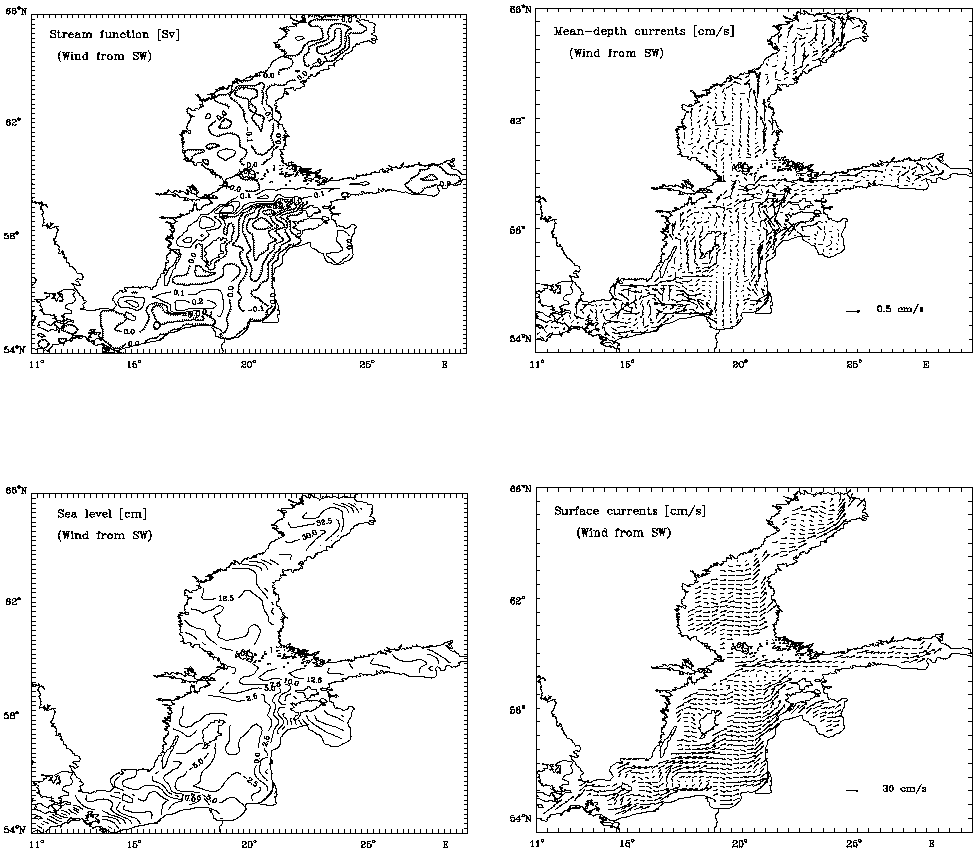

Figure 17: Stream function for mass transport [Sv], mean - depth currents [cm/s], sea level [cm] and surface currents [cm/s] for the strong wind of constant velocity blowing from Suthwest. The hatched areas in stream function distributions indicate the regions of counterclockwise (cyclonic) water circulation.

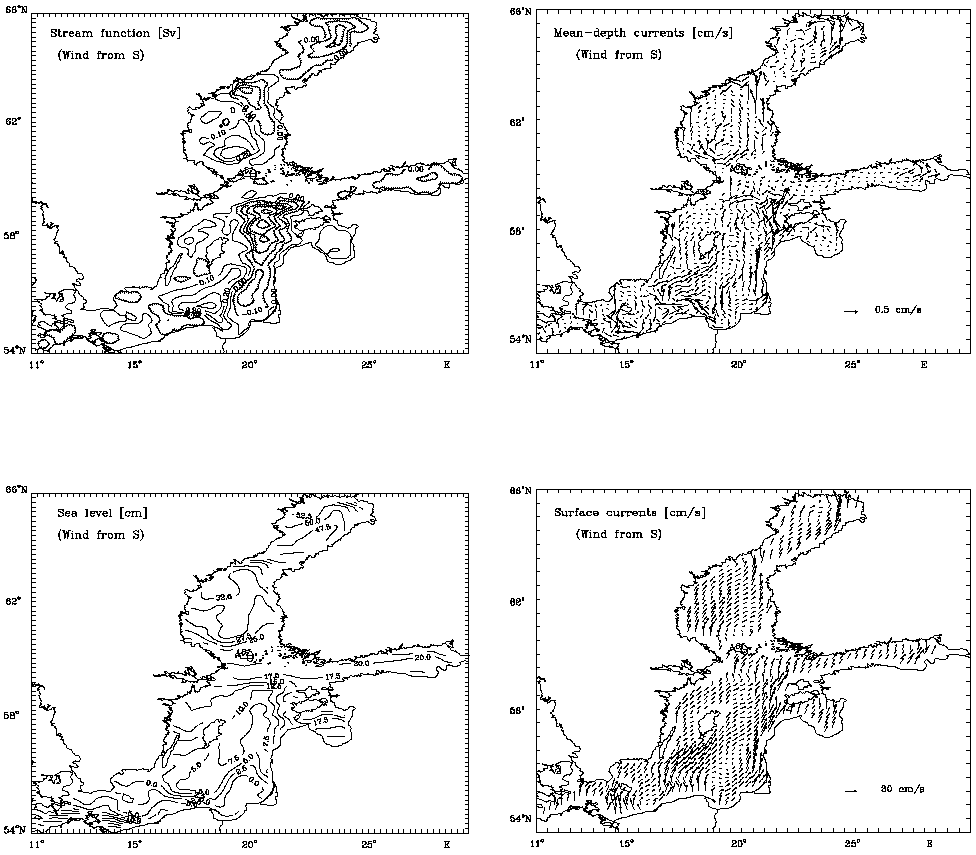

Figure 18: Stream function for mass transport [Sv], mean - depth currents [cm/s], sea level [cm] and surface currents [cm/s] for the strong wind of constant velocity blowing from South. The hatched areas in stream function distributions indicate the regions of counterclockwise (cyclonic) water circulation.

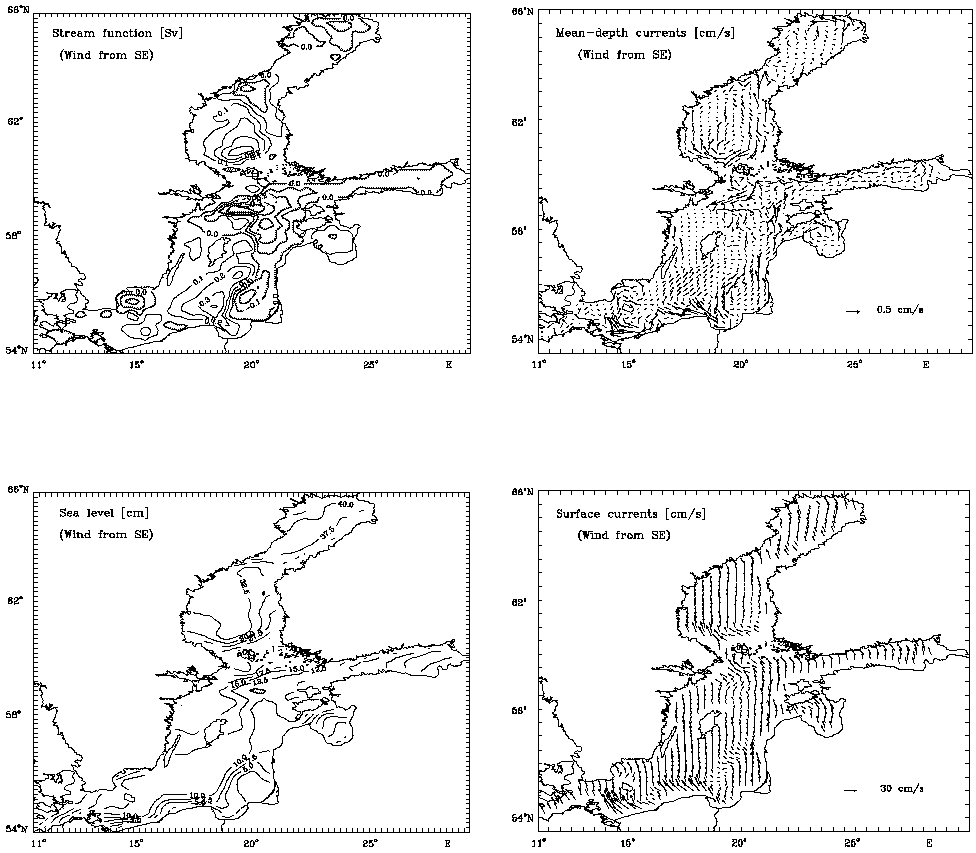

Figure 19: Stream function for mass transport [Sv], mean - depth currents [cm/s], sea level [cm] and surface currents [cm/s] for the strong wind of constant velocity blowing from Southeast. The hatched areas in stream function distributions indicate the regions of counterclockwise (cyclonic) water circulation.

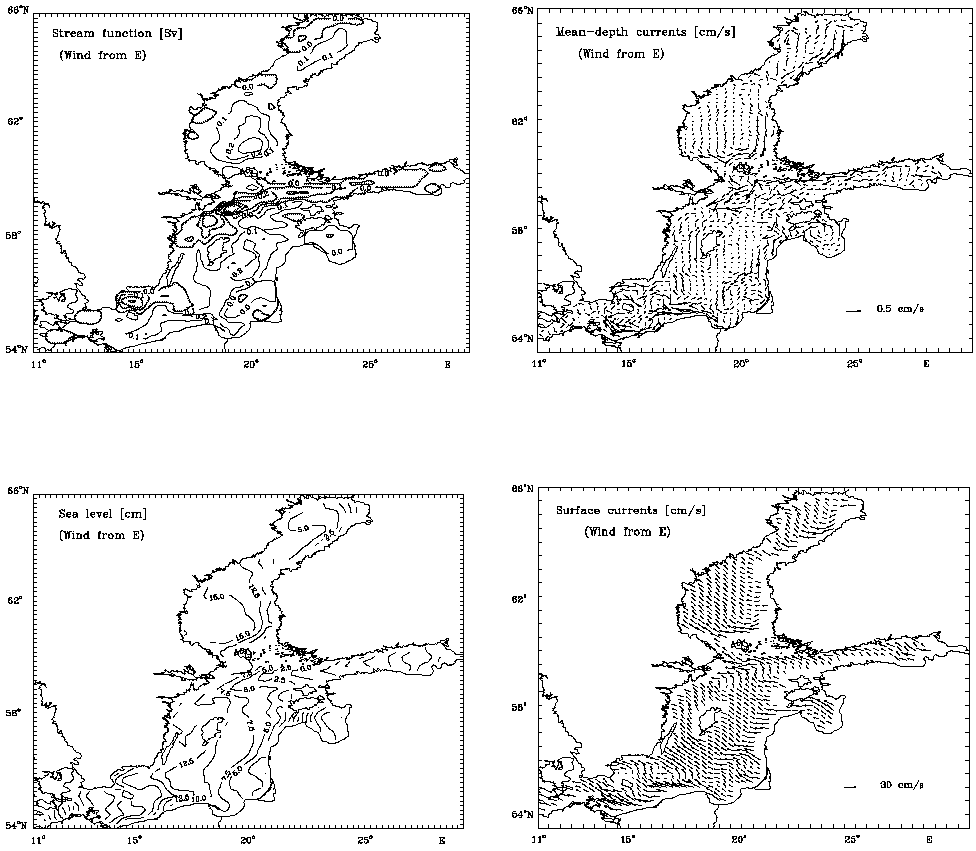

Figure 20: Stream function for mass transport [Sv], mean - depth currents [cm/s], sea level [cm] and surface currents [cm/s] for the strong wind of constant velocity blowing from East. The hatched areas in stream function distributions indicate the regions of counterclockwise (cyclonic) water circulation.

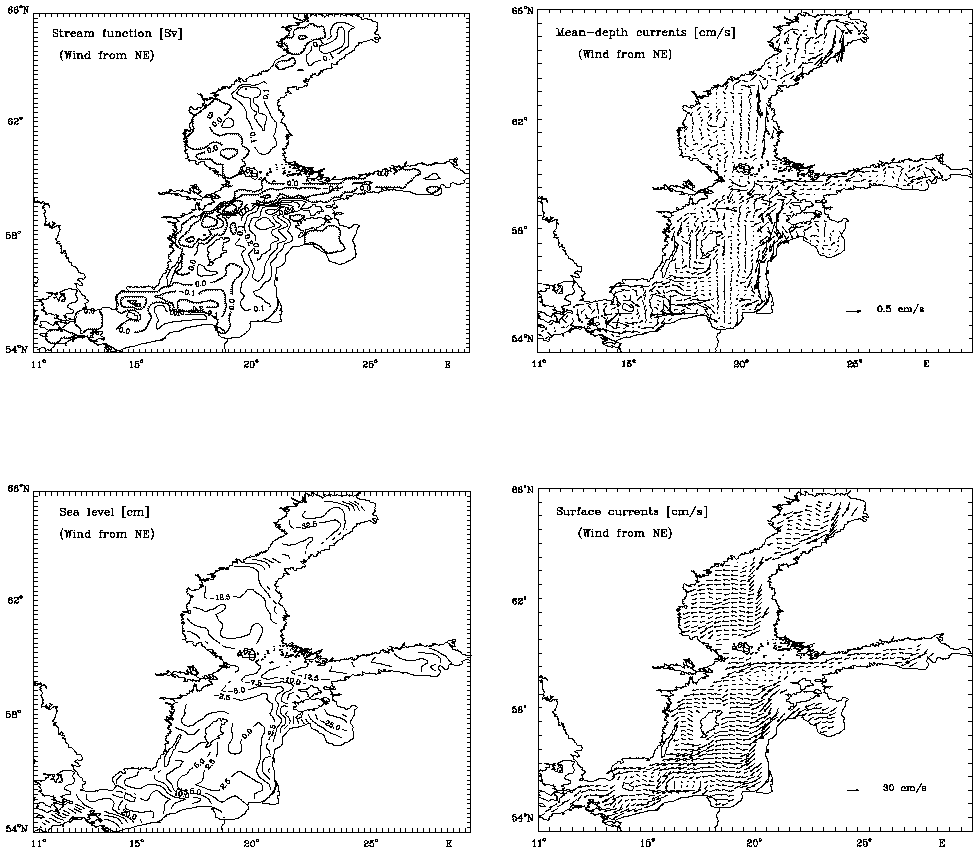

Figure 21: Stream function for mass transport [Sv], mean - depth currents [cm/s], sea level [cm] and surface currents [cm/s] for the strong wind of constant velocity blowing from Northeast. The hatched areas in stream function distributions indicate the regions of counterclockwise (cyclonic) water circulation.